ENVIRONMENTAL RESEARCH
COMMUNICATIONS

PAPER • OPEN ACCESS

Cloud condensation nuclei characteristics at the Southern Great Plains site: role of particle size distribution and aerosol hygroscopicity

To cite this article: Piyushkumar N Patel and Jonathan H Jiang 2021 *Environ. Res. Commun.* **3** 075002

Environmental Research Communications

PAPER

Cloud condensation nuclei characteristics at the Southern Great Plains site: role of particle size distribution and aerosol hygroscopicity

Piyushkumar N Patel[1,2,*] **and Jonathan H Jiang**[1,*]

[1] Jet Propulsion Laboratory, California Institute of Technology, Pasadena, CA, United States of America
[2] Universities Space Research Association, Columbia, MD, United States of America
[*] Authors to whom any correspondence should be addressed.

E-mail: piyushkumar.n.patel@jpl.nasa.gov **and** Jonathan.H.Jiang@jpl.nasa.gov

OPEN ACCESS

RECEIVED
29 March 2021

REVISED
15 June 2021

ACCEPTED FOR PUBLICATION
23 June 2021

PUBLISHED
5 July 2021

Keywords: cloud condensation nuclei, aerosol, supersaturation, hygroscopicity, closure analysis

Supplementary material for this article is available online

Abstract

The activation ability of aerosols as cloud condensation nuclei (CCN) is crucial in climate and hydrological cycle studies, but their properties are not well known. We investigated the long-term measurements of atmospheric aerosol properties, CCN concentrations (N_{CCN}) at supersaturation (SS = 0.1%–1.0%), and hygroscopicity at the Department of Energy's Southern Great Plains (SGP) site to illustrate the dependence of N_{CCN} on aerosol properties and transport pathways. Cluster analysis was applied to the back trajectories of air masses to investigate their respective source regions. The results showed that aged biomass burning aerosols from Central America were characterized by higher accumulation mode particles (N_{accu}; median value 805 cm^{-3}) and relatively high aerosol hygroscopicity (κ; median value ~0.25) values that result in the higher CCN activation and relatively high N_{CCN} (median value 258–1578 cm^{-3} at a SS of 0.1%–1.0%). Aerosols from the Gulf of Mexico were characterized by higher N_{accu} (~35%), and N_{CCN} (230–1721 cm^{-3} at a SS of 0.1%–1.0%) with the lowest κ (~0.17). In contrast, relatively high nucleation mode particles (N_{nucl}; ~20%) and low N_{CCN} (128–1553 cm^{-3} at a SS of 0.1%–1.0%) with higher κ (~0.30) values were observed on the aerosols associated with a westerly wind. The results indicate particle size as the most critical factor influencing the ability of aerosols to activate, whereas the effect of chemical composition was secondary. Our CCN closure analysis suggests that chemical composition and mixing state information are more crucial at lower SS, whereas at higher SS, most particles become activated regardless of their chemical composition and size. This study affirms that soluble organic fraction information is required at higher SS for better N_{CCN} prediction, but both the soluble organics fraction and mixing state are vital to reduce the N_{CCN} prediction uncertainty at lower SS.

1. Introduction

Suspended atmospheric aerosols allow for the water vapor condensation under certain supersaturation (SS) conditions and subsequently evolve into cloud droplets by serving as cloud condensation nuclei (CCN). Changes in the amount or the CCN properties will indirectly affect the climate by perturbing the cloud development and precipitation (Rosenfeld *et al* 2008, Li *et al* 2011). In this sense, the CCN concentration is an important parameter affecting aerosol-cloud interaction. The radiative forcing induced by aerosol-cloud interaction ($-0.55 \pm 0.63\ Wm^{-2}$) is larger than the one induced by aerosol-radiation interaction ($-0.27 \pm 0.50\ Wm^{-2}$) (IPCC 2014). Moreover, the uncertainty in the radiative forcing associated with the aerosol-cloud interaction remains high and is significantly larger than that associated with the aerosol-radiation interaction (IPCC 2014). Despite the considerable efforts to better understand aerosol-cloud interaction during the last decade, the uncertainty associated with the radiative forcing due to aerosol-cloud interaction has not

decreased significantly (Seinfeld *et al* 2016). Reducing this uncertainty is crucial for increasing our confidence in predictions of global and regional climate models (IPCC 2014). The fundamental parameter relevant for understanding the aerosol-cloud interaction is the CCN (Rosenfeld *et al* 2014). Hence, the significant uncertainty in aerosol-cloud interaction points to the necessity of dedicated observational and modelling efforts to improve the scientific understanding of CCN activation and accurately quantify the aerosol perturbed change in cloud microphysics (Rosenfeld *et al* 2014).

The ability of particles to act as CCN is mainly controlled by aerosol particle size following by chemical composition (Dusek *et al* 2006) and meteorological conditions (i.e., supersaturation (SS) and uplift force of air parcels; Seinfeld & Pandis 2016). CCN are particles directly emitted (as primary particles) into the atmosphere from natural and anthropogenic sources (Després *et al* 2012, Duan *et al* 2018) or aerosol particles that have undergone growth processes and possible chemical transformation in the atmosphere. These fine particles may originate from atmospheric new particle formation (NPF) events, anthropogenic combustion, or other various emission sources (Paasonen *et al* 2018). With the development and dissemination of techniques, measurements of ambient aerosol size distribution and chemical composition have increased in the last few decades. However, the global coverage of such data is still far from sufficient (Fan *et al* 2016), and the effort to systematically combine surface measurement sites is only at its earliest stages. Earlier studies suggested that measuring the aerosol hygroscopicity under subsaturated water vapor conditions has been proposed as a way to estimate the CCN activity of aerosols (Brechtel & Kreidenweis 2000, Kreidenweis *et al* 2005). In those studies, particle hygroscopicity was used to predict the critical supersaturation or critical diameter of particles, above which the thermodynamic equilibrium between the aerosols and the surrounding vapor collapses and the vapor condensation rate exceeds the evaporation rate. This leads to the continuous growth of the particles, which are thus solution droplets. The advancement of a single parameter κ that incorporates Raoult's law and the Kelvin effect with the given value of surface tension of water made the quantitative comparison between hygroscopicity at subsaturated condition and CCN activation more feasible (Petters & Kreidenweis, 2007). Information on CCN number concentration (N_{CCN}) at specific SS values is needed for the present-day climate models. To fulfill this requirement, many attempts have been made to retrieve N_{CCN} from aerosol hygroscopicity and size measurements at various regions such as the Amazon rainforest (Gunthe *et al* 2009, Pöhlker *et al* 2016), rural continental sites (Dusek *et al* 2006, Cho Cheung *et al* 2020), large cities (Lance *et al* 2009, Rose *et al* 2010), coastal locations (Dusek *et al* 2003, Gong *et al* 2020) and subarctic (Kammermann *et al* 2010). Several investigations have raised attention to the effect of aerosol mixing state on N_{CCN} (Ervens *et al* 2010, Wang *et al* 2010, Wex *et al* 2010). However, hygroscopicity data for ambient aerosols is still far from sufficient (Swietlicki *et al* 2008).

The Atmospheric Radiation Measurement (ARM) program initiated by the US Department of Energy (DOE) aims to improve the parameterization of clouds in global climate models (Stokes & Schwartz 1994). The Southern Great Plains (SGP) site under the ARM program is one of the world's largest and most extensive climate research facilities, which has over 20 years of long-term ground-based measurements of aerosol and cloud properties (Ackerman & Stokes 2003, Dong *et al* 2005). While the SGP site is located in a rural environment, around 40 km away from the nearest population centers, it is influenced by a mixture of anthropogenic, biogenic, and biomass burning aerosol sources along with long-range transported aerosols. Indeed, earlier studies showed a distinct seasonal variability in size and composition of aerosols, aided by favorable air masses at the SGP (Parworth *et al* 2015, Logan *et al* 2018). Therefore, it provides a unique platform to investigate the role of aerosol in CCN activity extensively. The prevailing aerosols at the ARM-SGP site typically contain organic and black carbon associated with biomass burning and inorganic aerosols composed of sulfate and nitrate species (Parworth *et al* 2015, Logan *et al* 2018). None of the prior studies at the SGP site demonstrated the differences in intrinsic hygroscopicity among those aerosol species and their roles in aerosol activation processes. Thus, this study aimed to characterize the variation in aerosol hygroscopicity and CCN activity under the influence of different air mass histories by utilizing a long, continuous record (January-December, 2019) of aerosol properties and CCN concentration measured at the SGP site. Section-1 outlines the methodology, instrumentation, and observations used in this study. Section-2 provides the present study results, which cover identifying the aerosol source regions and associated variation in aerosol characteristics and their activation processes. Section-3 summarizes the key findings of the present study and discusses areas of focus for future research.

2. Experiments & data analysis

2.1. Site description and measurements

The present study utilizes comprehensive *in situ* measurements conducted at the ARM-SGP extended central facility (E13) (36.605 °N 97.486 °W) site located in a mixed land-use area of cattle pastures and agricultural fields in Lamont, Oklahoma, U.S. (https://www.arm.gov/capabilities/observatories/sgp). The central facility

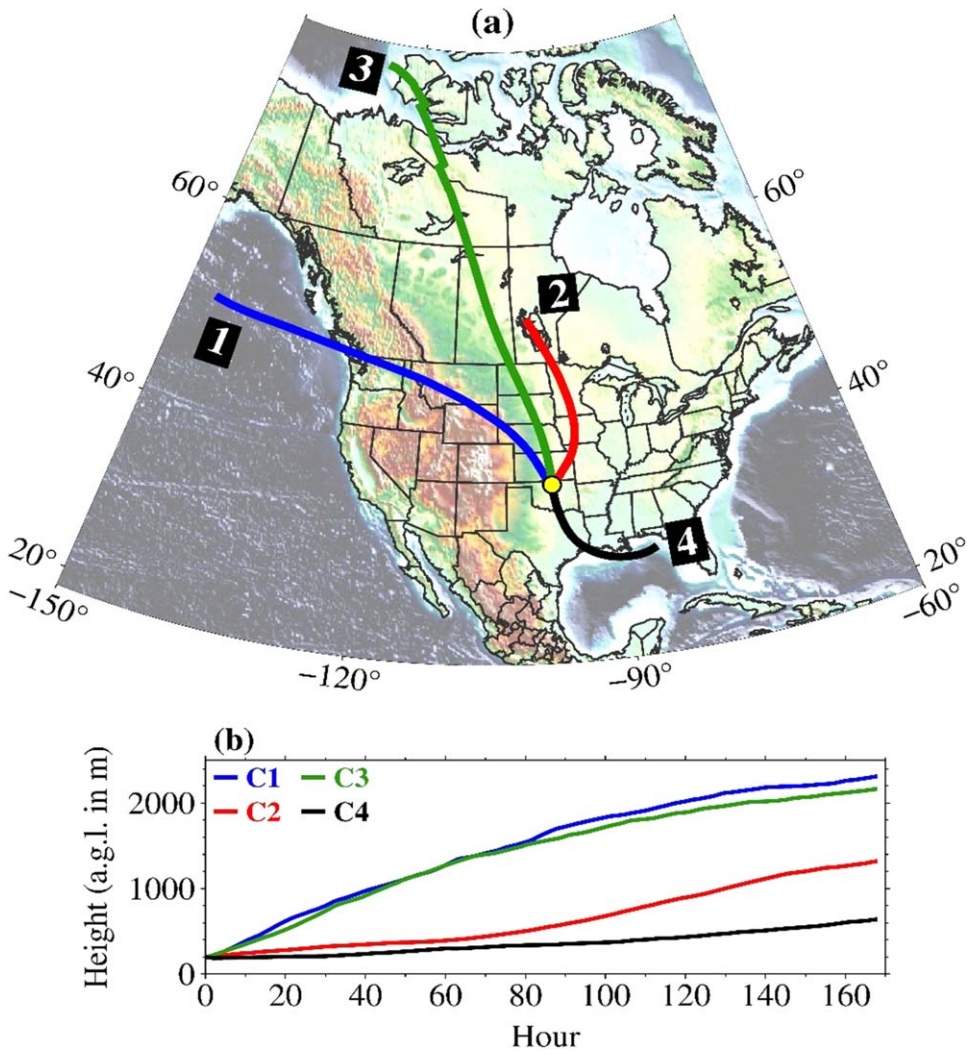

Figure 1. Cluster classification of 168 h (a) back trajectories during measurement period, and (b) airmass heights are shown in the graph below. Airmasses with both C2 and C4 have slow movements and relatively from the lower elevation, which originated from the Central America and Gulf of Mexico, respectively. While airmass in C1 and C3 are associated with the intercontinental long-range transportation from the high elevation.

Table 1. List of instruments, measured quantities, manufacturer, and data period (used in this study).

Instrument	Measurement	Manufacture/Model	Data period (used in this study)
Scanning Mobility Particle Sizer (SMPS)	Size Distribution from 10 nm to 512 nm	TSI Inc. 3936	January-December 2019
Dual Column Cloud Condensation Nuclei Counter (CCNC)	CCN concentration at a various set of supersaturations (0.1%, 0.2%, 0.4%, 0.8%, 1.0%)	Droplet Measurement Technologies CCN-200	January-December 2019
Condensation Particle Counter (CPC)	Concentration of condensation nuclei	TSI Inc. 3772	January-December 2019
Aerosol Chemical Speciation Monitor (ACSM)	Chemical composition (organics, ions of sulfate, nitrate, ammonium, and chloride)	Aerodyne Research Inc.	April-December 2019

employs surface-based instruments and remote sensing equipment that can provide continuous measurements of the physical and chemical properties of atmospheric constituents and local meteorological environments. The climate at the site is continental, with cold winters and hot summers. The site is impacted by various air masses originating from Central America, the Gulf of Mexico, and influence from long-range transport (figure 1 & Figure S1 (available online at stacks.iop.org/ERC/3/075002/mmedia)) with accompanying diversity in aerosol concentrations and properties. The site experiences complex and highly variable aerosol chemical compositions

Table 2. Statistics on the occurrence of respective airmass clusters for each month during the study period.

Month	Cluster 1	Cluster 2	Cluster 3	Cluster 4	Undefined
January	81 (43.5%)[a]	53 (28.5%)	46 (24.7%)	6 (3.2%)	0 (0.0%)
February	45 (26.8%)	91 (54.2%)	16 (9.5%)	15 (8.9%)	1 (0.6%)
March	74 (39.8%)	68 (36.6%)	31 (16.7%)	13 (7.0%)	0 (0.0%)
April	54 (30.0%)	92 (51.1%)	12 (6.7%)	22 (12.2%)	0 (0.0%)
May	21 (11.3%)	55 (29.6%)	6 (3.2%)	74 (39.8%)	30 (16.1%)
June	27 (15.0%)	18 (10.0%)	13 (7.2%)	122 (67.8%)	0 (0.0%)
July	8 (4.3%)	55 (29.6%)	8 (4.3%)	85 (45.7%)	30 (16.1%)
August	13 (7.0%)	23 (12.4%)	0 (0.0%)	150 (80.6%)	0 (0.0%)
September	10 (5.6%)	13 (7.2%)	0 (0.0%)	133 (73.9%)	24 (13.3%)
October	82 (44.1%)	37 (19.9%)	45 (24.2%)	22 (11.8%)	0 (0.0%)
November	77 (42.8%)	19 (10.6%)	43 (23.9%)	16 (8.9%)	25 (13.9%)
December	88 (47.3%)	50 (26.9%)	9 (4.8%)	39 (21.0%)	0 (0.0%)
All data	580 (26.5%)	574 (26.2%)	229 (10.5%)	697 (31.8%)	110 (5%)

[a] The number indicates the total number of trajectories associated with particular cluster (percentage contribution from particular cluster)

with time and particle size, as reflected in that of growth factor (GF) described by Mahish & Collins, (2017). The ARM-based Aerosol Observation System (AOS) has several ground-based instruments that can retrieve aerosol physical and chemical properties at the lowest atmospheric levels. Table 1 lists the routine aerosol measurements at the site that were used for the analysis presented here. All datasets used for this analysis are available for download from the ARM archive (https://adc.arm.gov/).

The scanning mobility particle sizer (SMPS) measured dry particle number size distribution (PNSD) with a TSI 3936 SMPS at 5 min interval. The SMPS system consisted of an electrostatic classifier with a differential mobility analyzer (DMA) and a TSI 3772 CPC. A total of 109 bins were used to measure a diameter range from 10.6 nm to 512 nm. A sheath to aerosol flow ratio of 5:1 was used for the DMA. An additional diffusion correction for the inlet tube was applied, assuming a laminar flow (Hinds 1999). Before deployment, the sizing accuracy of the SMPS was confirmed using the National Institute of Standards and Technology (NIST)-certified polystyrene latex spheres. Total particle number concentrations for particles larger than 10 nm in diameter were obtained from the condensation particle counter (CPC). A CPC, which has a ~10% detection efficiency for particles of 10 nm diameter, was connected to the same inlet as the SMPS. The additional details about the calibration, operation, accuracy, and uncertainty of both instruments are discussed elsewhere (Kuang 2016a, 2016b). N_{CCN} was measured using a continuous-flow, streamwise thermal gradient dual-column cloud condensation nuclei counter (CCNC). The sampled aerosol particles are guided within a sheath flow through this chamber and can become activated to droplets, depending on the supersaturation conditions and particles ability to act as CCN. Dual-column CCNC has two columns to measure different samples at different supersaturations (SS) simultaneously. During the experiment, one column measures CCN concentration for fixed value of supersaturation (ss $=$ 0.4% in the present study), whereas second column measures CCN concentration at 5 different supersaturation conditions (0.1%, 0.2% 0.4%, 0.8% and 1.0%). The additional description about the operation, calibration, data quality, and uncertainty is discussed elsewhere (Uin 2016).

The Aerosol Chemical Speciation Monitort (ACSM) employs thermal vaporization, electron impact ionization mass spectrometer that can measure ground-level species, such as organics (carbonaceous compounds), ions of nitrate, sulfate, ammonium, and chloride, in units of $\mu g\ m^{-3}$ (Ng *et al* 2011). ACSM, in conjunction with the other measurement platforms and air mass trajectory analysis, provides crucial information about the air mass pathways and potential aerosol sources over regions. More detail about ACSM measurements are given elsewhere (Watson *et al* 2018, 2020).

2.2. Derivation of the particle hygroscopicity parameter (κ)

Firstly, the N_{CCN} and total particle number concentration (N_{CN}) data were synchronized into 5-minute averages, which corresponded to the time interval for particle size distribution data measured by SMPS. According to Köhler theory (Köhler 1936), whether or not an aerosol particle can act as a CCN is primarily controlled by its size, chemical composition, and maximum supersaturation in its vicinity. The aerosol hygroscopicity (κ) values in the present study were derived using κ-Köhler theory (Petters & Kreidenweis 2007) using CCN activity data (κ_{CCN}). For $\kappa_{CCN} > 0.1$, the following approximate expressions can be used, assuming the surface tension of the examined solution droplets ($\sigma_{s/a}$) is that of pure water:

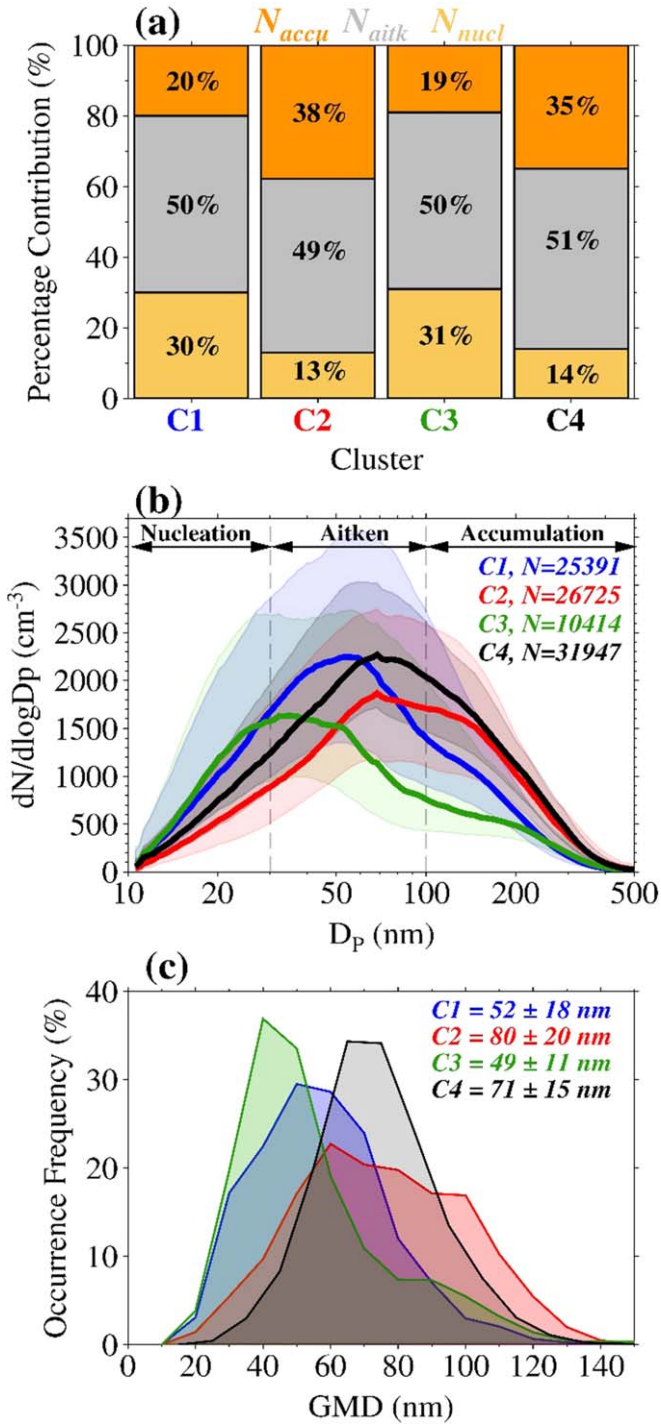

Figure 2. (a) Percentage contribution in the nucleation, Aitken and accumulation mode particles for all four clusters. (b) The median of particle number size distribution associated with derived four airmass clusters during the study period, where shaded area shows the first and third quartiles. The total number of size distribution spectra used in each cluster throughout the study period is denoted as N in the figure. The gray dashed line separates out the nucleation, Aitken and accumulation modes. (c) frequency distribution of the geometric mean diameter of the aerosol system during all four airmass clusters along with mean value of GMD for each cluster has mentioned.

$$\kappa_{CCN} = \frac{4A^3}{27 d_{crit}^3 ln^2 S} \tag{1}$$

with

$$A = \frac{4\sigma_{s/a} M_w}{RT\rho_w} \tag{2}$$

where d_{crit} is the critical diameter above which all particles are activated into droplets for a certain supersaturation ratio, S (= supersaturation+1). M_w and ρ_w are the molecular weight and water density, while R

Table 3. Parameters for each mode of the fitted lognormal distributions for the number size distributions for all four clusters shown in figure 2. N_0 represents the total number concentration within the mode (cm^{-3}), the value in bracket shows the median value of particle number concentrations for respective mode and cluster, D_m is the median diameters (μm) and σ_g represents the geometric standard deviation.

	Cluster 1 (C1)	Cluster 2 (C2)	Cluster 3 (C3)	Cluster 4 (C4)
Nucleation Mode				
N_0	34653 (830)	13156 (428)	26991 (960)	17440 (598)
D_m	0.04524	0.04452	0.04362	0.04438
σ_g	1.25	1.24	1.25	1.24
Aitken Mode				
N_0	57753 (2047)	49587 (1659)	43535 (1443)	63530 (2052)
D_m	0.10916	0.12312	0.1012	0.12066
σ_g	1.44	1.41	1.51	1.42
Accumulation Mode				
N_0	23102 (448)	38455 (805)	16543 (399)	43599 (905)
D_m	0.29308	0.31116	0.3232	0.3095
σ_g	1.41	1.40	1.54	1.53
Total				
N_0	115508 (1046)	101198 (903)	87069 (705)	124569 (1147)
D_m	0.1098	0.15788	0.08924	0.14624
σ_g	2.25	2.14	2.64	2.19

and T are the ideal gas constant and the absolute temperature, respectively. Simultaneously measured N_{CCN} and PNSDs were used to derive d_{crit} using the approach described by Rose *et al* (2008) and Mei *et al* (2013).

Additionally, a simple mixing rule on chemical volume fractions for an assumed internal mixture proposed by Petters & Kreidenweis (2007) is used to calculated κ_{chem}:

$$\kappa_{chem} = \sum_i \varepsilon_i \kappa_i \tag{3}$$

Where ε_i and κ_i are the volume fraction and hygroscopicity parameter, respectively, for the individual (dry) chemical components, and i is the number of components in the mixture. The ACSM measured bulk composition is used to calculate κ_{chem} in the present analysis. The ACSM-measured aerosol components mainly consisted of organics, $(NH_4)_2SO_4$, and NH_4NO_3 (Zhang *et al* 2014, Zhang *et al* 2016). The κ values for $(NH_4)_2SO_4$, and NH_4NO_3 are 0.67 and 0.61, respectively, which are derived from previous laboratory experiments (Petters & Kreidenweis 2007). The linear function derived by Mei *et al* (2013) was used to estimate κ_{org} ($= 2.10 \times f_{44}$–0.11) in our study, where f44 is the fraction of $m/z = 44$ in total organics. The particle hygroscopicity is thus the volume average of the participating species. Volume fractions of species were derived from mass concentrations and densities of the participating species. The densities of NH_4NO_3 and $(NH_4)_2SO_4$ are 1720 kg m^{-3} and 1770 kg m^{-3}, respectively. The density of organics is assumed to be 1200 kg m^{-3} (Turpin & Lim, 2001). More detailed descriptions of the method to derive κ_{chem} can be found elsewhere (Zhang *et al* 2014).

Additionally, to remove the outliers in κ data, we defined an outlier by values larger or smaller than 1.5 times the interquartile range (IQR) as follows:

$$Q1 - 1.5 * IQR \; or \; Q3 + 1.5 * IQR \tag{4}$$

Where Q1 and Q3 are the first and third quarters of kappa data and IQR is Q3 minus Q1. About 7% of the data has been removed, according to equation (4).

3. Results & discussions

3.1. Identification of air mass origins and potential source regions

In order to assess the potential origin of air masses that affect aerosols characteristics during the study period, seven-days air mass back trajectories over study location were calculated every 4 h using the National Oceanic and Atmospheric Administration (NOAA) Air Resources Laboratory Hybrid Single-Particle Lagrangian Integrated Trajectory (HYSPLIT) for the entire sampling period (Stein *et al* 2015). For the analysis, a model is initiated with the six-hourly Global Data Assimilation System (GDAS) archived data with a resolution of 1° in longitude and latitude. The endpoint of the trajectories was 200 m a.g.l. (above ground level) at the ARM-SGP

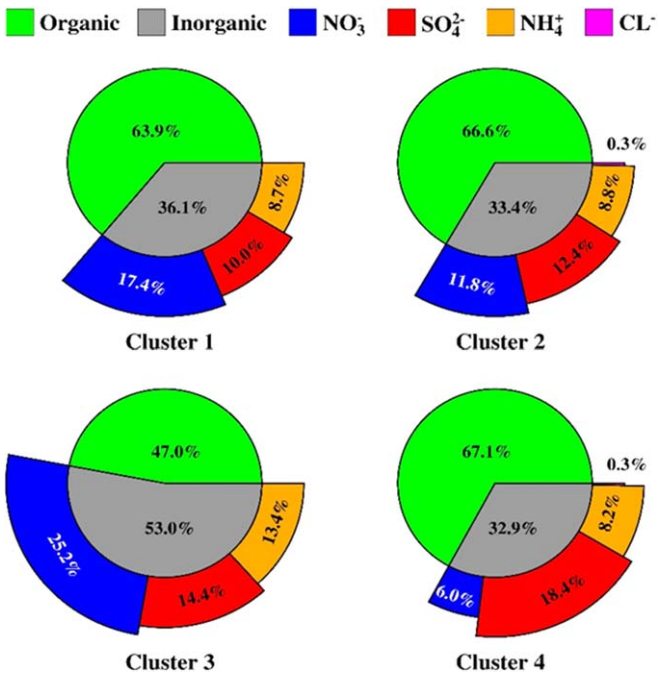

Figure 3. Percentage fraction of various chemical components of aerosol particles measured by ACSM at the ARM-SGP site for all four air mass histories during April-December, 2019. The inner pie chart illustrates the percentage fraction of organic and inorganics components, while outer pie chart demonstrates the percentage fraction from subspecies of inorganics.

site. These back trajectories from various sources (Figure S1) were classified into clusters using the cluster analysis technique (Dorling *et al* 1992). This analysis resulted in four distinct air mass back trajectory clusters (see figure 1; hereafter referred to as C1, C2, C3, and C4). Month wise occurrence frequency of each cluster is listed in table 2. Synoptic and mesoscale dynamics play essential roles in governing the movement of the air masses that transport aerosols from their sources to the SGP site (Parworth *et al* 2015, Logan *et al* 2018). The high-elevated air mass cluster C1 is associated with a westerly wind, contributing ~27% of the total back trajectories, bringing air masses from the arid and mixed forest regions in the west of the SGP site. The intercontinental transport from Asia (mainly from eastern China) has also been seen during C1, mainly containing land-based anthropogenic aerosols (Lin *et al* 2014). Like C1, C3 also shows long-range transport from Canada, mainly influenced by continental emissions, contributing the least (~11%) to total back trajectories. This set of trajectories also originates from the northern plain, passed over grassland and cropland (Trishchenko *et al* 2004), and is influenced by weak biogenic emissions (Liu *et al* 2020). Both C1 and C3 mostly dominate during late Fall and Winter. Unlike C1 and C3, most back trajectories during C2 and C4 are low-elevated and transport from shorter distances, depending on the position of high- and low-pressure systems passing through the region. During C2, the air masses arriving at the SGP site primarily originated from Central America, dominated during spring, contributing ~26% of the total back trajectories. This set of trajectories are primarily attributed to agricultural burns and wildfires in Central America (Peppler *et al* 2000, Wang *et al* 2009). During C4, air mass arriving at the SGP site originated primarily from the southern region, contributing the highest (~32%) to the total back trajectories. During summer, these trajectories were passed by urban/industrial areas such as Oklahoma City and eastern Texas, which are influenced mainly by anthropogenic emissions. A fraction of trajectories during C4 pass over the biogenic-rich emissions regions southeast of the SGP site. This indicates that biogenic emissions likely contribute to secondary organic aerosol mass at SGP (Parworth *et al* 2015, Liu *et al* 2020). Previous studies reported that a set of back trajectories associated with air mass cluster C4, having a signature of biomass burning smoke aerosols (especially during spring) and transport of marine air masses from the Gulf of Mexico (Parworth *et al* 2015, Logan *et al* 2018, Liu *et al* 2020). The pollution and smoke aerosols tend to be confined closer to the surface during moist, stagnant conditions, while the processes between the interface of the free troposphere and boundary layer, such as subsidence, entrainment, and turbulent, settle down the long-range transported aerosols to the surface (Logan *et al* 2014, Dong *et al* 2015).

3.2. Aerosol physical and chemical characteristics

Particles of different sizes have different formation routes, sources, and behaviors. Therefore, the simultaneous observations of aerosol particle number size distributions are co-located to various air mass clusters and further

Table 4. Statistics of ACSM-measured aerosol chemical composition at the ARM-SGP sie during April-December, 2019. Measurement units are $\mu g\ m^{-3}$ for all species.

	Cluster 1				Cluster 2			
	mean	median	25th percentile	75th percentile	mean	median	25th percentile	75th percentile
Organic	1.40	1.14	0.68	1.82	2.24	1.91	0.92	3.07
Nitrate	0.38	0.20	0.10	0.46	0.40	0.22	0.12	0.43
Sulfate	0.22	0.17	0.10	0.29	0.42	0.31	0.18	0.58
Ammonium	0.19	0.14	0.07	0.24	0.30	0.21	0.11	0.37
Chloride	0.00	0.00	0.00	0.01	0.01	0.01	0.00	0.01
	Cluster 3				Cluster 4			
	mean	median	25th percentile	75th percentile	mean	median	25th percentile	75th percentile
Organic	0.95	0.74	0.47	1.07	2.55	2.37	1.70	3.22
Nitrate	0.51	0.34	0.18	0.61	0.23	0.17	0.12	0.26
Sulfate	0.29	0.24	0.16	0.38	0.70	0.66	0.35	0.95
Ammonium	0.27	0.22	0.13	0.35	0.31	0.28	0.16	0.41
Chloride	0.00	0.00	0.00	0.01	0.01	0.01	0.00	0.01

divided into the subsets to examine their dependence on the air mass origin. Figure 2(b) represents the corresponding median particle number size distributions for all four air mass clusters. The shaded area indicates the range between the 25th and 75th percentiles. To better understand the particle size modes, we fitted the particle number size distribution (PNSD) to three lognormal functions. The parameterization function for lognormal distribution is as follows (Seinfeld & Pandis 2016):

$$N(\ln D_p) = \frac{dN}{d\ \log D_p} = \sum_{i=1}^{n} \frac{N_0}{\sqrt{2\pi}\ \log_{10}\sigma_g^i} \exp\left(-\frac{(\log_{10} D_p - \log_{10} D_m)^2}{2(\log_{10}\sigma_g^i)^2}\right), \quad (5)$$

N_0 is the total particle number concentration (in cm^{-3}) of the ith mode, σ_g is the geometric standard deviation of the ith mode distribution, and D_m is the median diameter (in μm) of the ith mode. Every PNSD was individually parameterized by a trimodal distribution, where the number of I = 1,2,3 represents the nucleation, Aitken, and accumulation mode, respectively. Nucleation mode (N_{nucl}) is that particles observed below 30 nm, Aitken mode (N_{aitk}) is that from 30 to 100 nm, and accumulation mode (N_{accu}) is that beyond 100 nm (Ueda *et al* 2016, Willis *et al* 2016). For each PNSD, we searched for an optimal fitting function until the coefficient of determination was larger than 0.97. The parameters for the number size distribution (N_0, D_m, σ_g) for each of the three size ranges are shown in table 3. PNSDs resemble those show three modes, i.e., nucleation, Aitken, and accumulation modes, which can be distinguished, as shown in figure 2(b). While similarities are evident in the size distribution's shapes and modes, several differences between the clusters can be seen in figure 2. The average relative contribution of the particle number concentration in the three modes for individual air mass clusters is shown in figure 2(a). Figure 2(b) represents the corresponding median particle number size distributions for all four air mass clusters. The shaded area indicates the range between the 25th and 75th percentiles. The frequency distribution of geometric mean diameter (GMD) for each air mass cluster, along with the mean GMD values, is shown in figure 2(c).

Variations in the contributions of the particle modes during the observational period indicated a potential difference in the particle characteristics over the region during the four distinct air mass histories. In general, the PNSD exhibited a bimodal distribution for all four air mass clusters with varying degrees of particle concentration. The median PNSDs during C1 and C3 have the first peak at below 50 nm and the second at > 100 nm. In these periods, the majority (50%) of the aerosol particles were present in the Aitken mode and least (~14%) in the accumulation mode. Interestingly, a prominent presence of nucleation mode particles (~30%) was also observed during both the environment even though the air mass history varies. It also reflects in the frequency distribution of GMD, spreading towards the lower size range with the mean values 52 nm (C1) and 49 nm (C3). Changes in GMD of the PNSD for a given observation site most likely reflect the different particle emission sources and aging histories. Moreover, the relatively lower occurrence frequency of C3 (table 2) contributes significantly lower to total aerosol number concentration with a median value of 705 cm^{-3}. On the other hand, C1 had a second maximum contribution to total aerosol number concentrations (median value of 1046 cm^{-3}). In general, nucleation mode particles are produced by homogeneous and heterogeneous nucleation processes, formed during natural gas-to-particle condensation. Nucleation mode particles are transferred to the Aitken mode through coagulation of nucleation particles, condensation of vapors onto existing particles (Seinfeld & Pandis 2016), or cloud processing (Hoppel *et al* 1994), during which they grow into that size range.

Table 5. Cluster-wise statistics for the number concentrations of CCN (N_{CCN}) and total particles (N_{CN}) and activation ratio (AR) under five different supersaturation conditions along with median values of critical diameter (d_{crit}) and hygroscopicity parameter (κ_{CCN}) during the study period.

		Median values (cluster wise)			
	SS (%)	**C1**	**C2**	**C3**	**C4**
N_{CCN} (cm^{-3})	0.1%	128	258	134	230
	0.2%	466	701	313	669
	0.4%	883	1095	573	1136
	0.8%	1389	1456	954	1578
	1.0%	1553	1578	1057	1721
N_{CN} (cm^{-3})		2874	2572	2329	3169
d_{crit}		70.0	68.0	75.1	68.7
κ_{CCN}		0.30	0.25	0.22	0.17

Unlike C1 & C3, the PNSD are entirely different during the C2 & C4, as seen in figure 2(a). We observed that, while Aitken mode particles still dominated the particle number concentration, the accumulation mode exhibited an increase in particle number concentration during C2 (38%) and C4 (35%). The Aitken mode peak was observed at ~70 nm, and the accumulation mode peaked at >150 nm. The consistent presence of such particles is seen as the spread of the distribution of the GMD in figure 2(c), with the mean GMD values 80 nm (C2) and 71 nm (C4). Additionally, C4 contributes highest to the total aerosol number concentration than the other air mass clusters, with a median value of 1147 cm^{-3}, followed by C2 with a median value of 903 cm^{-3}. Accumulation mode particles are mostly emitted to the atmosphere from natural sources, e.g. mineral dust, marine aerosol or bioaerosols, mainly long-range transported or more aged aerosols. These results are similar to the previous studies (Andrews *et al* 2011, Marinescu *et al* 2019). Moreover, the new particle formation (NPF) event is the primary source of secondary aerosol particles. This could significantly increase the number concentrations of nucleation mode particles, and those particles are growing into Aitken and/or accumulation mode size ranges and last for a few hours until they disappear into the atmospheric condensation and coagulation sinks (Dal Maso *et al* 2005). Therefore, the occurrence frequency of NPF has been investigated during each air mass environment (Figure S2) to find their contribution to total particle concentration. In total, 205 NPF events were visually identified by following the protocol given in Kulmala *et al* (2012) during the entire study period. The investigation reported that NPF occurred more frequently during C1 (~36%) may significantly contribute to nucleation mode particles. Interestingly, the occasional NPF occurrence during C3 (~12%) suggests that nucleation mode particles are associated with long-range transportation via the westerly wind from Asia. The observation shows that NPF occurrence frequency during C2 (20%) and C4 (29%) may contribute to nucleation mode particles.

According to Köhler's theory, particle activation depends on their solubility for particles of constant size, which is a function of their composition, including the number of potential solute molecules and their solubility. Therefore, we analyzed the ACSM-measured bulk chemical composition of aerosol particles, reaching the study location via different air mass histories. Figure 3 gives the mass fraction of organics, ammonium, chloride, nitrate, and sulfate as measured by ACSM, and the average mass concentration of these components is summarized in table 4 during April-December, 2019. Organic aerosols (OA) contributed the most considerable fraction to the total mass concentration during C1, C2, and C4 periods, accounting for >60% on average, whereas inorganics were greater than 50% of the total mass during C3. Sulfate was abundant in absolute mass during C4 with an average concentration of 0.7 $\mu g\,m^{-3}$. In contrast, nitrate is dominated in C3 (mean concentration 0.51 $\mu g\,m^{-3}$) and C1 (mean concentration 0.38 $\mu g\,m^{-3}$). The nitrate mass was lowest during C4 (mean concentration 0.23 $\mu g\,m^{-3}$) than others due to its semi-volatile behavior pushing the equilibrium back to the gas phase with warmer temperatures. Moreover, cations and anions illustrate a good correlation (Figure S3), but during C4, ammonium is insufficient for full neutralization of the anions, suggesting the aerosols associated with air mass cluster C4 were more acidic. In general, ammonium nitrate will not partition into the condensed phase until particulate sulfate is fully neutralized (Guo *et al* 2017). Thus, the more acidic behavior of aerosol might be another explanation for the lower nitrate during C4. These given values might have slight variation due to incomplete datasets of aerosol chemical composition, but the variation in chemical composition associate with air mass clusters are almost similar in comparison to previous studies (Parworth *et al* 2015, Mahish *et al* 2018, Liu *et al* 2020). Subsequently, we used these measurements for the computation of the chemical-based hygroscopicity parameter (κ_{chem}) and the further evaluation of CCN closure analysis (discussed in the following section).

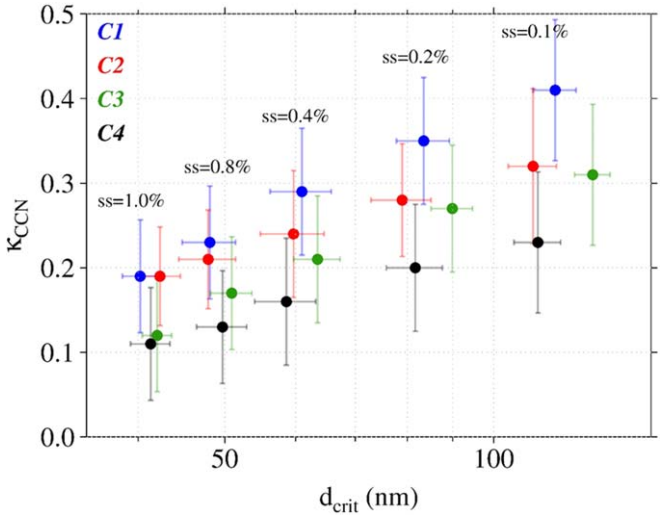

Figure 4. Size dependence of the hygroscopic parameter (κ_{CCN}) for every SS level are plotted against their corresponding critical diameter. Dots represent the median value and the bars represent the interquartile range. The colors indicate the various air mass clusters. A clear size dependence and trends in κ_{CCN} levels can be observed.

3.3. CCN concentration and aerosol hygroscopicity

Statistics for the number concentration of cloud condensation nuclei (N_{CCN}) and total particles (N_{CN}) as well as for critical diameter (d_{crit}) and kappa (κ_{CCN}) values under specific supersaturation conditions for different air mass history are summarized in table 5. The N_{CN} amount represents the total number of boundary layer aerosols that can serve as centers for condensation, while the N_{CCN} is the fraction of N_{CN} that can activate as CCN. The median N_{CCN} values exhibited large variability throughout the study period, ranging from 128 to 1721 cm^{-3} for a supersaturation value of 0.1%-1.0%. The peak values of N_{CCN} observed in C4 (median 230–1721 cm^{-3} at a SS of 0.1%–1.0%) and C2 (median 258–1578 cm^{-3} at a SS of 0.1%–1.0%) suggesting a large number of hygroscopic particles transported to the observational site from Gulf of Mexico (South) and Central America (North), respectively. The particles associated with C4 and C2 that are advected to the SGP site tend to readily activate as CCN under moist environments brought about by mesoscale and synoptic weather events (Logan *et al* 2018, 2020). The relatively low air mass occurrence frequency of C3 could have contributed lowest to N_{CN} (median 2329 cm^{-3}) and N_{CCN} (median 134–1057 cm^{-3} at a SS of 0.1%–1.0%). Though the N_{CN} (median 2874 cm^{-3}) is higher in C1, a low concentration of hygroscopic aerosols was inferred from the decrease in N_{CCN} (median 128–1553 cm^{-3} at a SS of 0.1%–1.0%). A further discussion on how the variability in the particle characteristics affects their activation is presented in section 2.4. Furthermore, CCN spectra (plotted against the supersaturation) are a frequently used representation in various studies to summarize the observed N_{CCN} values over the cloud-relevant supersaturation range for a given period and location (Gunthe *et al* 2009, Pöhlker *et al* 2016). The dependence of N_{CCN} on supersaturation is shown by plotting the averages of the measured N_{CCN} during different air mass histories at the specific supersaturations of the CCN counters (Figure S4). A logarithmic function fits better to the data in all these different environments than the power function $N_{CCN}(SS) = C^*(SS)^k$. It is not a new observation that the power function is not perfect for expressing the N_{CCN} versus SS relationship. Previous studies have used other function types, for instance, an exponential function (Mircea *et al* 2005, Deng *et al* 2013), a product of the hypergeometric and power function (Cohard *et al* 1998, Pinsky *et al* 2012), and the error function (Dusek *et al* 2006, Pöhlker *et al* 2016). More than 95% of cases in the current observations show a high correlation coefficient ($R > 0.98$) with logarithmic function fit.

The median d_{crit} and associated κ_{CCN} value calculated for the observation period ranged from 40.2 to 129.1 nm and 0.11 to 0.41 (under supersaturation 0.1%–1.0%), respectively, which exhibited larger variations than that reported in the previous literature from the various sites across the world (Gong *et al* 2019, Hung *et al* 2014, Iwamoto *et al* 2016, Meng *et al* 2014; references therein). The large variability in κ_{CCN} values measured at the ARM-SGP station compared to the previous studies may be attributed to the shorter measurement period, while the present study lasted for one year and thereby was subject to seasonal variations. Moreover, the adaptation of κ estimation methodology also observed a large variation in the κ_{CCN} values. However, the κ_{CCN} was computed using d_{crit} in the present study, representing the average hygroscopicity of the aerosols (Rose *et al* 2008). Nevertheless, the aerosol composition at the SGP station are frequently influenced by regional emissions and long-range transported natural and anthropogenic aerosols through different seasons, as indicated in previous studies (Andrews *et al* 2011, Parworth *et al* 2015, Marinescu *et al* 2019); hence this elucidates the large variability

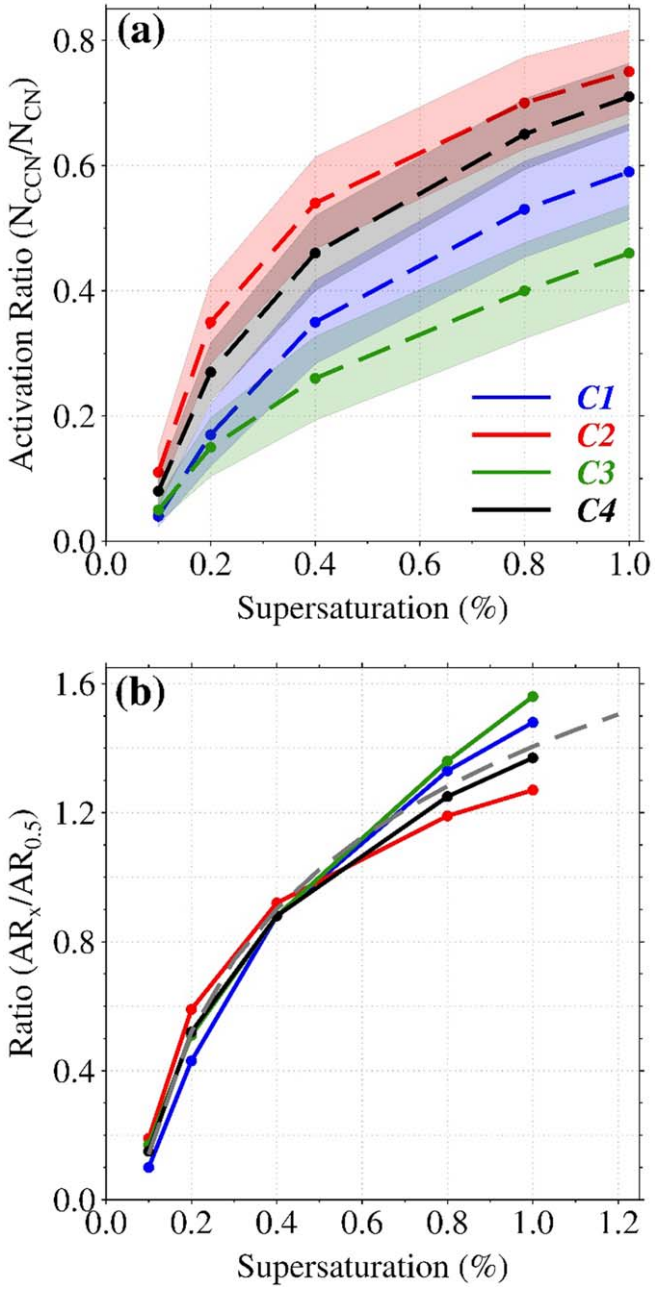

Figure 5. (a) Variation of CCN activation ratio (AR) at different SS during all four air mass histories. shaded area indicates the standard error. (b) Ratio of activations ratios for all SS over the activation ratio at 0.5% SS for each air mass clusters based on particle size distribution $>$ 10 nm. At SS $=$ 0.5% (x-axis) ratio is 1. The gray dotted line is the average fit through all curves, whereby y $=$ A*ln (SS %) $+$ b with A $=$ 0.55 $\pm$ 0.02 and b=1.41 $\pm$ 0.02.

in κ_{CCN} values observed in this study. Furthermore, the median values of κ_{CCN} against their corresponding d_{crit} for different air mass histories is shown in figure 4. The error bars represent the interquartile range of κ_{CCN}. Both κ_{CCN} and d_{crit} decrease with an increase of supersaturation, suggesting that the chemical composition was not uniform among sizes. Smaller particles tended to have lower κ_{CCN} values corresponding to less hygroscopic species, while more hygroscopic species in larger ones. These low κ_{CCN} values in smaller diameter suggest the presence of organic material, which has also been observed in previous studies (Parworth *et al* 2015, Mahish & Collins 2017, Liu *et al* 2020). This observed trend was consistent with the assumption that larger particles are activated first. Although the Kelvin effect may cause some decrease of κ with decreasing particle size, this effect is small, less than 5% for particles in the diameter ranged from 50–200 nm (Swietlicki *et al* 2008, Wang *et al* 2018). Moreover, κ_{CCN} values are higher during C1 and lowest during C4. Due to incomplete datasets of aerosol chemical composition, we were unable to determine the higher κ_{CCN} values in C1 directly. However, the previous studies reported that the increased hygroscopicity is probably associated with the promotion of condensation of semi-volatile species such as ammonium nitrate and semi-volatile organic species due to a

combination of shallow boundary layers, enhanced emissions, and low temperature (Parworth *et al* 2015). Moreover, during C1, a relatively high concentration of hydrophobic particles such as dust and organic soil particles from crop harvesting contribute to be depression of κ_{CCN} of larger particles (Mahish & Collins, 2017). Conversely, the highest organic mass concentration from biomass burning and anthropogenic emissions during C4 further reduces the κ_{CCN} values. During C2, the biomass burning aerosol contribute a significant fraction of the organic aerosol that oxidize to a more water-soluble form, likely due to aging occurring during the transport (Parworth *et al* 2015, Liu *et al* 2020), resulting in relatively high value of hygroscopicity. Particles in this size range are mostly accumulation mode and have undergone cloud processing and aging. In comparison of C2, κ_{CCN} is relatively low in C4, likely due to aerosol during C2 are more aged than C4 (Liu *et al* 2020). Interestingly, the presence of high inorganic concentration in comparison to organic during C3 still have lowest κ_{CCN} than other air mass clusters, likely due to coating of hydrophobic particles such as carbonaceous particles associated to intercontinental transportation that suppress the overall hygroscopicity of particle. Furthermore, the κ_{CCN} curve against size is found flatter during C2 and C4 in comparison to C1 and C3, likely due to the presence of more aged and chemically homogenous aerosols.

Besides, the comparison of mean κ_{chem} with that derived from the N_{CCN} (κ_{CCN}) measurements against the aerosol particle size is shown in Figure S5. Here, κ_{chem} is computed from the bulk chemical composition, whereas κ_{CCN} is arithmetic based on measurements of particles with a diameter range from 10 nm to 512 nm. As illustrated in Figure S5, the κ_{chem} calculated from equation (3) agreed well with the measured κ_{CCN} and having a similar trend. The difference between κ_{chem} and κ_{CCN} is statistically insignificant at all diameters during C3 and C4, while the one during C1 and C2 became statically significant, particularly at larger particle sizes. This large difference in C1 and C2 (more frequent during winter and spring) can be due to incomplete aerosol chemical composition datasets (only available during April-December). Although the ACSM-based κ_{chem} may overestimate particle hygroscopicity because of its sensitivity to larger particles, the mean κ_{chem} is lower than κ_{CCN}. One possible explanation for the lower κ_{chem} is uncertainty in the hygroscopicity of organic aerosols because it is assumed to be a simple linear function of f44 (Mei *et al* 2013). Because the coefficients in the linear function κ_{org} ($= 2.10 \times f_{44}$-0.11) are based on measurements in different regions, they may not fit the aerosols sampled during the present study. Another cause may be the particle aging/coating process, for instance, condensation of secondary aerosol on preexisting particles. The resulting particle hygroscopicity may depend more on the coating layer than on the preexisting particle composition (Ma *et al* 2013).

3.4. CCN activation

The fraction of aerosol particles acting as CCN at a given supersaturation is known as the CCN activation ration/fraction (AR) and is a crucial parameter for characterizing the CCN activity (Dusek *et al* 2006, Andreae, 2009). Figure 5(a) shows a direct comparison of the AR spectra for the given SS segregated to various air mass histories for the period of interest, which reveals characteristics differences in the curve's shape. The observed differences among the AR spectra in figure 5(a) reflect some of the significant trends in the aerosol variability in SGP. In general, the key parameters in the CCN activation behavior are aerosol number size distribution (primary) and, in a secondary role, the chemical composition of particles (Dusek *et al* 2006). Thus, the cluster-wise averaged PNSD (in figure 2) and κ_{CCN} (in figure 4) have to be considered to explain the different shapes in figure 5(a). Focusing on C2 and C4, it can be stated that with increasing SS, the d_{crit} decreases and is shifted from the accumulation-mode towards the Aitken-mode size range. Thus, comparatively small SS levels can already activate most particles of the pronounced accumulation mode. In contrast, during C1 and C3, while the same SS levels still activate the accumulation mode remains inactivated. It means that the ratio of Aitken and accumulation-mode particles determine the activated fraction as a function of SS and thus also the steepness of the activation spectra in figure 5(a). During C2 and C4, 50% of particles activate at 0.4% SS, while in the cases of C1 and C3, 50% activation occurs at SS $=$ 0.8% and 1.0%, respectively, reveling that the ratio of Aitken and accumulation-mode particles determine the activated fraction as a function of SS and thus also the steepness of the activation spectra. While size appears as the dominant parameter in the particle activation behavior, in certain cases variability in chemical composition also matters. In figure 5(a), this can be seen between C2 and C4. In the presence of more aged aerosol in C2, the 50% activation occurs already at SS $=$ 0.32% than to be C4 (SS $=$ 0.44%) behavior. While figure 2(a) shows that the relatively higher accumulation mode presence during C4 than C2, the observed difference in figure 5(a) can be explained by the deviations in the corresponding κ_{CCN} size distribution (figure 4). In other words, the elevated κ_{CCN} during the intrusion of more aged aerosols in C2 allows the activation of particle sizes that remains inactivated at the lower κ_{CCN} levels in the C4 due to relatively larger contribution of organic aerosols. Therefore, the difference in chemical composition can explain the decreased SS in C2 and C4 cases. Furthermore, the lower κ_{CCN} would yield a larger d_{crit} or higher critical SS, and thus a lower CCN and cloud droplet concentration, which will turn lead to uncertainty in evaluating the

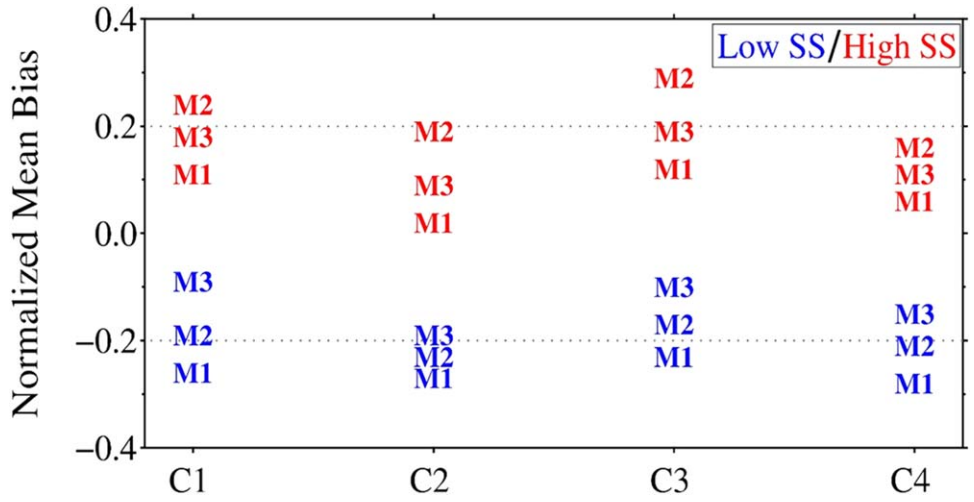

Figure 6. Normalized mean bias resulting from CCN closure analysis performed for all four air mass histories using three different parameterization methods. A value of 0.2 is equivalent to an average overprediction of 20%. M1 indicates the experimental average hygroscopicity method, M2 indicates the bulk chemical composition with internal mixing method and M3 indicates the bulk chemical composition with external mixing method.

Table 6. Fitting results of measured and predicted CCN concentrations. The values are the slope and R^2 (in brackets).

		C1	C2	C3	C4
0.1%	M1	0.79 (0.87)	0.81 (0.91)	0.75 (0.88)	0.80 (0.91)
	M2	0.82 (0.89)	0.83 (0.90)	0.79 (0.90)	0.82 (0.91)
	M3	0.87 (0.91)	0.89 (0.93)	0.83 (0.91)	0.87 (0.92)
0.2%	M1	0.80 (0.89)	0.82 (0.90)	0.78 (0.90)	0.81 (0.91)
	M2	0.84 (0.87)	0.86 (0.91)	0.83 (0.88)	0.85 (0.91)
	M3	0.91 (0.91)	0.90 (0.93)	0.85 (0.91)	0.91 (0.92)
0.4%	M1	0.83 (0.89)	0.84 (0.90)	0.83 (0.90)	0.83 (0.91)
	M2	0.88 (0.87)	0.86 (0.91)	0.91 (0.88)	0.86 (0.91)
	M3	0.94 (0.91)	0.92 (0.93)	0.93 (0.91)	0.91 (0.92)
0.8%	M1	1.01 (0.87)	1.01 (0.91)	1.02 (0.88)	1.01 (0.91)
	M2	1.06 (0.89)	1.06 (0.90)	1.07 (0.90)	1.05 (0.91)
	M3	1.04 (0.91)	1.04 (0.93)	1.05 (0.91)	1.05 (0.92)
1.0%	M1	1.06 (0.91)	1.04 (0.93)	1.01 (0.91)	1.04 (0.92)
	M2	1.14 (0.89)	1.12 (0.90)	1.10 (0.90)	1.09 (0.91)
	M3	1.11 (0.87)	1.09 (0.91)	1.07 (0.88)	1.11 (0.91)

associated aerosol indirect effects on clouds and climate. Contrary, the higher κ_{CCN} would accordingly result in a smaller d_{crit} or lower critical SS, and consequently higher estimated CCN and cloud droplet concentration.

We calculated the activation ratio (AR) for each measured SS based on the particle number size distribution >10 nm to compare the particle activation behaviors from various air mass clusters. Further, we computed the AR ratio at each SS (AR_X) to AR at SS = 0.5% ($AR_{0.5}$) to assess the changes in AR with respect to SS. In this study, N_{CCN} at SS = 0.5% were not measured directly therefore, the value was linearly interpolated. The result of the analysis is shown in figure 5(b). The dashed gray line represents a logarithmic fit through all four curves. A steep slope represents that the aerosol particle population activation is sensitive to small changes in SS, while a flat slope describes that a further increase in SS would not have a significant influence on the AR. The curves in figure 5(b) suggest that particles at all four clusters have distinct activation properties with changing SS, reflecting the results shown in figure5(a). Particles observed in the C2 & C4 have a high steeper slope up to SS = 0.5% thereafter, the curves flatten, indicating that the aerosol particle population is relatively insensitive to higher SS and that most particles activate at SS = 0.5%. The frequency distribution of GMD for C2 & C4 in figure 2(c) suggests that most particles are larger than 70 nm which will already activate at SS lower than 0.5%. The previous study associated with the lower AR at higher SS link it to the influence of nearby biomass burning and hence smaller less hygroscopic particles (Pöhlker *et al* 2016). Furthermore, Gunthe *et al* (2009) have shown in their findings that particles with a smaller electrical mobility diameter are less hygroscopic than larger particles due to the difference in composition. The mass fraction of inorganic constituents is higher in larger

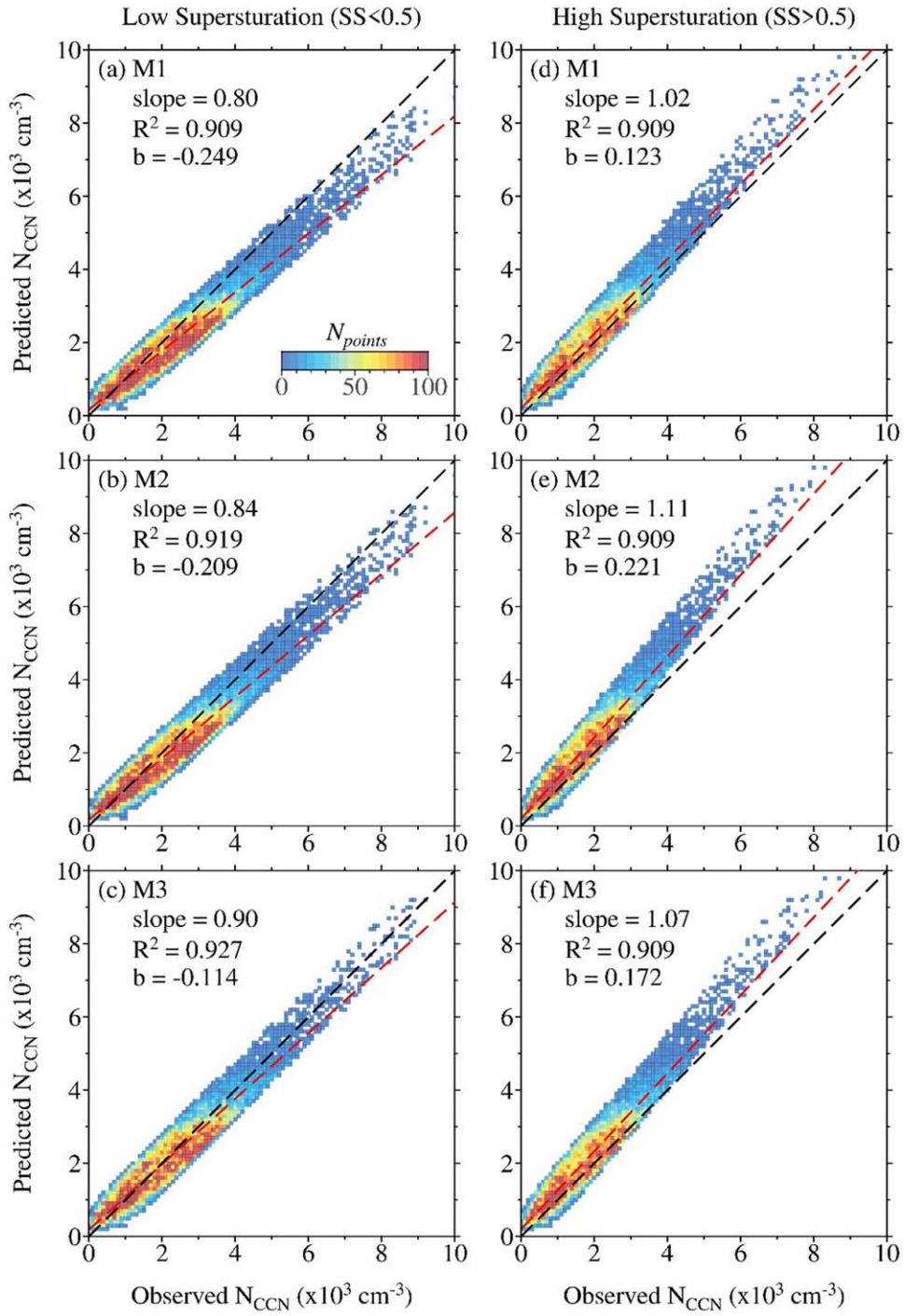

Figure 7. Density plots display the comparison of predicted and observed CCN concentration using (a) & (d) the experimental average hygroscopicity method, (b) & (e) the bulk chemcial composition with the assumptions of internal mixing method and (c) & (f) the bulk chemical compisition with the assumptions of external mixing method. Linear fit and the parameters are also shown. The black dash line indicates the unit slope (m = 1) line and red dashed line indicates the regression line.

particles (as seen in figure 3). Surprisingly, particle activation behavior in C2 (associated with pure continental signature) portrays that most particles active already at SS $<$ 0.4%, which is in line with the measured large particle sizes. It suggests that the mixing between water-solute organics and the natural (biogenic) sources leads to size distribution, which has hygroscopic behavior. Likewise, the mixing between biomass burning from the Gulf of Mexico and natural (marine) sources associated with C4 leads to a complex particle activation behavior and it is sensitive to SS $<$ 0.5%. Conversely, particle activation behavior in C1 & C3 is sensitive to higher SS, indicating the influence from long-range transported air pollution at the site. Regarding the C1, findings from a previous study (Lin *et al* 2014) showed that growing international trade in China exports a significant amount of air pollution to the USA, which highly contains land-based anthropogenic particles such as black carbon, carbon

monoxide, sulfate, etc (Lin *et al* 2014). These smaller anthropogenic particles (GMD = 57 nm; figure 2(c)) activate at higher SS greater than 0.5% due to less hygroscopic behavior of particles. Similarly, particles in C3, associated with transboundary transportation of land-based polluted particles, are sensitive to higher SS.

3.5. CCN Closure Analysis

Cloud resolving models require simple and efficient parameterizations of the complex microphysical basis to adequately reflect the spatiotemporal CCN cycling (Cohard *et al* 1998, Andreae 2009). The previous literature (Andreae 2009, Cai *et al* 2018, Deng *et al* 2013, Gunthe *et al* 2009, Jurányi *et al* 2011, Pöhlker *et al* 2016, Rose *et al* 2010 and references therein) reported several different schemes for the prediction of N_{CCN} to understand the involvement of size and chemical composition of aerosol particles in CCN activity under different environments, to improve the knowledge of aerosol-induced CCN activation further. Based on this fact, the present study used three different assumptions regarding particle diameter, chemical composition, and mixing state (internally & externally) for a CCN closure analysis.

(1) Using experimental average hygroscopicity (M1): in this scheme, the average hygroscopicity estimated using equation (1) represents the particle chemical composition and mixing state. However, it only represents the regional CCN activation due to aerosol hygroscopicity in SGP.

(2) Using bulk chemical composition and internally mixed (M2): in this scheme, the ACSM-based averaged chemical composition was assumed to be size-independent and internally mixed. All particles have an identical chemical composition in the entire size range.

(3) Using bulk chemical composition and externally mixed (M3): in this scheme, the aerosol chemical composition was assumed to be size-independent and externally mixed. There were three types of particles at each size: NH4NO3, (NH4)2SO4, and organics, and the concentrations of these three types of particles at each size were identical.

The κ-Köhler theory, as indicated in appendix-1, was used to calculate the critical diameter for the prediction of total N_{CCN}. Due to limited aerosol chemical composition datasets, a CCN closure analysis was performed during April-December, 2019. Table 6 describes the results of CCN closure for each airmass history. Closure analysis was assessed in terms of normalized mean bias (NMB $=\sum(CCN_{pre} - CCN_{mea})/\sum CCN_{mea}$), which represents the average N_{CCN} prediction error observed (Asa-Awuku *et al* 2011). Figure 6 shows the normalized mean bias of closure analysis for different airmass histories under low (SS $<$ 0.5) and high (SS $>$ 0.5) supersaturation conditions.

The fitting results depicted that M3 was more accurate than M2 at all SS values in all air mass histories, likely due to the internally mixed particles with homogenous composition had already grown into larger particles or activated as cloud droplets under high moist environments due to their hygroscopic nature. Simultaneously, heterogeneous reactions may have existed in the nucleation particle formation and the remaining particles were mainly externally mixed. The best CCN closure results were achieved in C2 and C4 compared to C3 and C1 in all the schemes, particularly for higher SS, possibly due to aged aerosols, which were less affected by assumptions of chemical composition and mixing state. A previous study conducted in Mexico City reported a similar pattern to that of C3 and C1, in which the presence of primary organic aerosols and black carbon in the form of an external mixture deteriorated the closure ratio (Wang *et al* 2010). The low concentration and simple species in C3 made the M3 scheme better for CCN prediction. Figure 6 illustrates that the N_{CCN} prediction accuracy using chemical methods (M2 & M3) depends on SS, typically underpredicting N_{CCN} at low SS but always overpredicting at high SS. This reflects the mean hygroscopicity derived from bulk chemical composition, usually higher than the hygroscopicity of smaller particles but lower than larger particles. In general, the mean hygroscopicity in chemical methods is closest to the hygroscopicity of particles with a d_{crit} of 100–130 nm, corresponding to SS of 0.1%–0.2%. However, the weak size-dependency of aerosol hygroscopicity due to particle aging neglected such an effect in C2 and C4 but expected to be prominent in C1 and C3 due to the strong size-dependency (as seen in figure 4). These results further confirm that the prediction of N_{CCN} is less sensitive to κ at high SS than at low SS and that the impact of hygroscopicity on the N_{CCN} prediction decreases with increasing SS. In addition, CCN closure is sensitive to solubility & surface tension of organics can lead to a poor closure ratio with a low-soluble inorganics fraction (Chang *et al* 2007). It is worth noting that the solubility of organics significantly affects CCN prediction in both external and internal mixing cases. The previous study in a region influenced by urban and industrial sources also suggested that knowledge of the water-soluble organic compound fraction combined with the assumptions of internally mixed aerosols can significantly improve CCN prediction (Asa-Awuku *et al* 2011). Notable underprediction of N_{CCN} is reduced (10%–15%) from C2 to C4 to C1 at lower SS when assuming external mixing, in agreement with the aerosol aging, which should lead to both oxidized organic aerosol and a

significant amount of internal mixing. This pattern indicates that at lower SS, the solubility of organics plays a crucial role in the CCN activity of aerosols, whereas at higher SS values, most particles become activated regardless of their chemical composition and size. In general, CCN closure error increases (15%–20%) as κ_{CCN} decreases (from C1 to C2 to C4) at lower SS, suggesting that detailed size-resolved composition and mixing states information is crucial for accurate prediction of N_{CCN}. The study conducted over the Northern Pacific Ocean (Schulze *et al* 2020) suggested that the environment with intense organic aerosol intrusion into the marine boundary layer similar to C4 are least likely to be precisely reproduced by regional models that need a detailed investigation of their particle characteristics, frequency, and the resulting impact on cloud properties is warranted.

Figure 7 illustrates the comparison of different prediction methods under low supersaturation (SS $<$ 0.5) and high supersaturation (SS $>$ 0.5) conditions irrespective of any airmass cluster. It was more reliable to assume that the external mixing method was more accurate than the internal mixing method at both low and high supersaturation environments. It is worth noting that the soluble organic fraction is required at higher SS, but both the soluble organics fraction and mixing state are substantial at lower SS for CCN prediction. As illustrated in figure 7, the predictions obtained from M1 were slightly poor than the chemical methods (M2 & M3), while at higher supersaturation, the M1 method was more robust. It suggests that the chemical method was still unreliable under high supersaturation due to the critical diameters of particles at high supersaturation being too small. The CCN closure error increases as SS decreases, particularly for M1, suggesting that detailed mixing state and size-resolved compositional information or both is critical for accurate CCN prediction. As the aerosol hygroscopicity calculation used in this study relies on an assumption of internal mixing of organic and inorganic aerosol components, it is difficult to determine whether CCN closure error results from external mixing of organic and inorganic aerosols or a result of variable composition with size. In general, the particle mixing state in the CCN closure studies has been considered size-independent, which may not be correct for all cases because the mixing state varies with the time of the day, aging of aerosols, and distance from the potential source. The atmospheric processes, such as coagulation, condensation, and photochemical transformation, shifts the externally mixed aerosols to an internally mixed state. Therefore, the better CCN closure results are unexpected by considering the long lifetime of externally mixed aerosols. Aerosol aging processes such as condensation, mass transfer processes, or reactive uptake cause the production of secondary species and reduce the overall contribution of primary species that further reduces error in CCN closure. It suggests that implementing an external mixing state, particularly for aged aerosols, is still valid in global climate models. However, it does not represent actual ambient conditions. Therefore, a knowledge of size-resolved chemical composition and the mixing state assumption is required to reduce the CCN closure error.

4. Summary and Discussion

The present study investigates aerosol characteristics and their ability to activate as CCN using measurements obtained over the ARM-SGP site. Measurements of aerosol properties were combined with cluster analysis of the back trajectories to gain insight into aerosol characteristics and their influence on CCN under various airmass environments. Trajectory analysis demonstrated that aerosols that prevail at SGP have major source regions: The Gulf of Mexico, Mexico, and Central America, along with long-range transportation. The characteristics of these airmass clusters and their contribution to CCN activation are as follows:

- Airmass transported from Central America (C2) was characterized by biomass burning aerosols, contributing highest to accumulation mode particles (~38%) with relatively high aerosol hygroscopicity (~0.25), likely due to the aging of aerosols. Aged aerosols with a GMD $>$ 80 nm and relatively high aerosol hygroscopicity (~0.25) demonstrates that ~50% of particles activate at SS $<$ 0.4%. It portrays both particle size and chemical composition together play a crucial role in the CCN activation.
- Airmass transported from the Gulf of Mexico (C4) has the signature of urban pollution, biomass burning smoke, and marine aerosols, contributing the highest to total particle concentration (~median value 1147 cm-3) and Naccu (~35%). The significant contribution from anthropogenic emissions reduces the aerosol hygroscopicity to the lowest (~0.17). Interestingly, even in the poor aerosol hygroscopicity condition, the relatively lower ratio of Aitken and accumulation mode particles increase the CCN activation ratio, and ~50% of particles activate at SS $<$ 0.5%. This demonstrates that particle size matters more than the chemical composition.
- High-elevated airmass associated with a westerly wind (C1) has a prominent presence of nucleation mode particles (~30%) and least contributes to accumulation mode particles (~19%) with a geometric mean diameter (GMD) $\sim$ 50 nm. Although the condensation of semi-volatile species under favorable meteorology

increases the aerosol hygroscopicity (0.30), the ~50% particle activation occurs at 0.8% SS. It suggests that CCN activation mainly depends on particle size followed by chemical composition.

- The minimal contribution from elevated airmass clusters (C3) from Canada to total have the lowest contribution to total particle contribution (median value 705 cm^{-3}) and relatively prominent contribution in fine mode particles (~20%). It mostly has a signature of continental aerosols, which are hygroscopically inactive, and ~50% activation occurs at 1.0% SS.
- The better association of biomass burning aerosols with CCN and accumulation mode aerosols during C2 indicates aerosols' aging process possibly enhanced the CCN activity prior to the marine airmass (C4). It suggests that particle size is responsible first, followed by chemical composition for the CCN activity.
- The CCN closure analysis indicates that the prediction method using bulk chemical composition is more reliable at lower SS. In contrast, the experimental average hygroscopicity method provides a robust prediction of NCCN at higher SS. Additionally, the external mixing method was more accurate than the internal mixing method at both low and high supersaturation environments. The solubility of organics plays a crucial role in the CCN activity of aerosols. The present closure analysis suggests that the soluble organic fraction is required at higher SS, but both the soluble organics fraction and mixing state are substantial at lower SS for better NCCN prediction. Finally, the closure error analysis suggests that detailed size-resolved compositional information and mixing state are critical to reducing the NCCN prediction uncertainty. This information will help establish the empirical hygroscopicity relationship for the climate models.

Acknowledgments

This work was conducted at the NASA-sponsored Jet Propulsion Laboratory (JPL), California Institute of Technology, under contract by NASA. We appreciate the facility provided by the JPL for data analysis and research. This work was supported by the NASA Postdoctoral Program, administered by Universities Space Research Association under contract with NASA. All data were obtained from the Atmospheric Radiation Measurement (ARM) Program sponsored by the U.S. Department of Energy, Office of Science, Office of Biological and Environmental Research, Climate and Environmental Sciences Division.

Data availability statement

All data that support the findings of this study are included within the article.

Appendix A1: N_{CCN} estimation in CCN closure analysis

The saturation ratio is given as follows:

$$S = a_w \exp\left(\frac{4\sigma M_w}{RT\rho_w D_p}\right) \tag{A1}$$

where a_w is the water activity of the solution droplet, σ is the surface tension of the solution, M_w and ρ_w are the molecular mass and density of water. R is the universal gas constant, and D_p is the size (Seinfeld & Pandis 2016). The critical diameter can be estimated from the Köhler theory based on its size distribution, chemical composition, and hygroscopic growth information. The critical diameter derived from the Köhler equation is as follows (Lance *et al* 2009):

$$d_{cri} = \left(\frac{27}{4}\left(\ln\left(\frac{S}{100}+1\right)\right)^2\left(\frac{\rho_w RT}{4\sigma M_w}\right)^3 \frac{M_w \rho_s \varepsilon_s \vartheta}{M_s \rho_w}\right)^{-1/3} \tag{A2}$$

Where ρ_s, M_s, and ϵ denote density, molecular mass, and volume fraction of the solute, respectively. ϑ is the effective van't Hoff factor. Assuming a pure internally mixed aerosol system with uniform composition, N_{CCN} can be predicted using the following equation based on the measured aerosol number size distribution and estimated critical diameter (Jurányi *et al* 2011):

$$N_{CCN} = \int_{d_{crit}}^{D_{max}} \left(\frac{dN}{dlogD_p}\right) dD_p \tag{A3}$$

The authors declare that they have no conflict of interest.

ORCID iDs

Piyushkumar N Patel https://orcid.org/0000-0003-2179-8739
Jonathan H Jiang https://orcid.org/0000-0002-5929-8951

References

Ackerman T P and Stokes G M 2003 The atmospheric radiation measurement program *Phys. Today* **56** 38–44
Andreae M O 2009 Correlation between cloud condensation nuclei concentration and aerosol optical thickness in remote and polluted regions *Atmos. Chem. Phys.* **9** 543–56
Andrews E, Sheridan P J and Ogren J A 2011 Seasonal differences in the vertical profiles of aerosol optical properties over rural Oklahoma *Atmos. Chem. Phys.* **11** 10661–76
Asa-Awuku A, Moore R H, Nenes A, Bahreini R, Holloway J S, Brock C A and Huey L G 2011 Airborne cloud condensation nuclei measurements during the 2006 Texas air quality study *Journal of Geophysical Research Atmospheres.* **116** 1–18
Brechtel F J and Kreidenweis S M 2000 Predicting particle critical supersaturation from hygroscopic growth measurements in the humidified TDMA. Part II: laboratory and ambient studies *J. Atmos. Sci.* **57** 1854–71
Cai M, Tan H, Chan C K, Qin Y, Xu H, Li F and Zhao J 2018 The size-resolved cloud condensation nuclei (CCN) activity and its prediction based on aerosol hygroscopicity and composition in the Pearl Delta River (PRD) region during wintertime 2014 *Atmos. Chem. Phys.* **18** 16419–37
Chang R Y W, Liu P S K, Leaitch W R and Abbatt J P D 2007 Comparison between measured and predicted CCN concentrations at Egbert, Ontario: Focus on the organic aerosol fraction at a semi-rural site *Atmos. Environ.* **41** 8172–82
Cho Cheung H, Chung-Kuang Chou C, Siu Lan Lee C, Kuo W C and Chang S C 2020 Hygroscopic properties and cloud condensation nuclei activity of atmospheric aerosols under the influences of Asian continental outflow and new particle formation at a coastal site in eastern Asia *Atmos. Chem. Phys.* **20** 5911–22
Cohard J M, Pinty J P and Bedos C 1998 Extending Twomey's analytical estimate of nucleated cloud droplet concentrations from CCN spectra *J. Atmos. Sci.* **55** 3348–57
Dal Maso M, Kulmala M, Riipinen I, Wagner R, Hussein T, Aalto P P and Lehtinen K E J 2005 Formation and growth of fresh atmospheric aerosols: Eight years of aerosol size distribution data from SMEAR II, Hyytiälä, Finland *Boreal Environ. Res.* **10** 323–36
Deng Z Z, Zhao C S, Ma N, Ran L, Zhou G Q, Lu D R and Zhou X J 2013 An examination of parameterizations for the CCN number concentration based on *in situ* measurements of aerosol activation properties in the North China Plain *Atmos. Chem. Phys.* **13** 6227–37
Després V R, Alex Huffman J, Burrows S M, Hoose C, Safatov A S, Buryak G and Jaenicke R 2012 Primary biological aerosol particles in the atmosphere: A review *Tellus, Series B: Chemical and Physical Meteorology.* **64** 1–58
Dong X, Minnis P and Xi B 2005 A climatology of midlatitude continental clouds from the ARM SGP central facility: Part I: Low-level cloud macrophysical, microphysical, and radiative properties *J. Clim.* **18** 1391–410
Dong X, Schwantes A C, Xi B and Wu P 2015 Investigation of the marine boundary layer cloud and CCN properties under coupled and decoupled conditions over the azores *J. Geophys. Res.* **120** 6179–91
Dorling S R, Davies T D and Pierce C E 1992 Cluster analysis: A technique for estimating the synoptic meteorological controls on air and precipitation chemistry-Method and applications *Atmospheric Environment Part A, General Topics.* **26** 2575–81
Duan J, Wang Y, Xie X, Li M, Tao J, Wu Y and Wang J 2018 Influence of pollutants on activity of aerosol cloud condensation nuclei (CCN) during pollution and post-rain periods in Guangzhou, southern China *Sci. Total Environ.* **642** 1008–19
Dusek U, Frank G P, Hildebrandt L, Curtius J, Schneider J, Walter S and Andreae M O 2006 Size matters more than chemistry for cloud-nucleating ability of aerosol particles *Science* **312** 1375–78
Dusek U, Covert D S, Wiedensohler A, Neusüss C, Weise D and Cantrell W 2003 Cloud condensation nuclei spectra derived from size distributions and hygroscopic properties of the aerosol in coastal south-west Portugal during ACE-2 *Tellus, Series B: Chemical and Physical Meteorology.* **55** 35–53
Ervens B, Cubison M J, Andrews E, Feingold G, Ogren J A, Jimenez J L and Allan J D 2010 CCN predictions using simplified assumptions of organic aerosol composition and mixing state: A synthesis from six different locations *Atmos. Chem. Phys.* **10** 4795–807
Fan J, Wang Y, Rosenfeld D and Liu X 2016 Review of aerosol–cloud interactions: mechanisms, significance, and challenges *J. Atmos. Sci.* **73** 4221–52
Gong X, Wex H, Müller T, Wiedensohler A, Höhler K, Kandler K and Stratmann F 2019 Characterization of aerosol properties at Cyprus, focusing on cloud condensation nuclei and ice-nucleating particles *Atmos. Chem. Phys.* **19** 10883–900
Gong X, Wex H, Voigtländer J, Wadinga Fomba K, Weinhold K, Van Pinxteren M and Stratmann F 2020 Characterization of aerosol particles at Cabo Verde close to sea level and at the cloud level: I. Particle number size distribution, cloud condensation nuclei and their origins *Atmos. Chem. Phys.* **20** 1431–49
Gunthe S S, King S M, Rose D, Chen Q, Roldin P, Farmer D K and Pöschl U 2009 Cloud condensation nuclei in pristine tropical rainforest air of Amazonia: Size-resolved measurements and modeling of atmospheric aerosol composition and CCN activity *Atmos. Chem. Phys.* **9** 7551–75
Guo H, Liu J, Froyd K D, Roberts J M, Veres P R, Hayes P L and Weber R J 2017 Fine particle pH and gas-particle phase partitioning of inorganic species in Pasadena, California, during the 2010 CalNex campaign *Atmos. Chem. Phys.* **171** 5703–19
Hinds W C 1999 *Aerosol Technology: Properties, Behavior, and Measurement of Airborne Particles.* 2nd edn (New Jersey, USA: John Wiley & Sons, Inc.) 978-0-471-19410-1
Hoppel W A, Frick G M, Fitzgerald J W and Larson R E 1994 Marine boundary layer measurements of new particle formation and the effects nonprecipitating clouds have on aerosol size distribution *J. Geophys. Res.* **99** 14443–59
Hung H M, Lu W J, Chen W N, Chang C C, Chou C C K and Lin P H 2014 Enhancement of the hygroscopicity parameter kappa of rural aerosols in northern Taiwan by anthropogenic emissions *Atmos. Environ.* **84** 78–87
IPCC 2014 :*Climate Change 2014: Synthesis Report. Contribution of Working Groups I, II and III to the Fifth Assessment Report of the Intergovernmental Panel on Climate Change [Core Writing Team, R.K. Pachauri and L.A. Meyer (eds.)]* (Geneva, Switzerland: IPCC) 978-92-9169-143-2 https://www.ipcc.ch/site/assets/uploads/2018/05/SYR_AR5_FINAL_full_wcover.pdf
Iwamoto Y, Kinouchi K, Watanabe K, Yamazaki N and Matsuki A 2016 Simultaneous measurement of CCN activity and chemical composition of fine-mode aerosols at noto Peninsula, Japan, in autumn 2012 *Aerosol Air Qual. Res.* **16** 2107–18

Jurányi Z, Gysel M, Weingartner E, Bukowiecki N, Kammermann L and Baltensperger U 2011 A 17 month climatology of the cloud condensation nuclei number concentration at the high alpine site Jungfraujoch *Journal of Geophysical Research Atmospheres.* **116** 1–16
Kammermann L, Gysel M, Weingartner E, Herich H, Cziczo D J, Holst T and Baltensperger U 2010 Subarctic atmospheric aerosol composition: 3. Measured and modeled properties of cloud condensation nuclei *Journal of Geophysical Research Atmospheres.* **115** 1–15
Köhler H 1936 The nucleus in and the growth of hygroscopic droplets *Trans. Faraday Soc.* **32** 1152–61
Kreidenweis S M, Koehler K, DeMott P J, Prenni A J, Carrico C and Ervens B 2005 Water activity and activation diameters from hygroscopicity data: I. Theory and application to inorganic salts *Atmos. Chem. Phys.* (https://doi.org/10.5194/acp-5-1357-2005)
Kuang C 2016a *Condensation Particle Counter (CPC) Instrument Handbook.* https://www.arm.gov/publications/tech_reports/handbooks/cpc_handbook.pdf (https://doi.org/DOE/SC-ARM-TR-145)
Kuang C 2016b *TSI Model 3936 Scanning Mobility Particle Spectrometer Instrument Handbook.* https://www.osti.gov/servlets/purl/1245993/ (https://doi.org/DOE/SC-ARM-TR-147)
Kulmala M, Petäjä T, Nieminen T, Sipilä M, Manninen H E, Lehtipalo K and Kerminen V M 2012 Measurement of the nucleation of atmospheric aerosol particles *Nat. Protoc.* **7** 1651–67
Lance S, Nenes A, Mazzoleni C, Dubey M K, Gates H, Varutbangkul V and Jonsson H H 2009 Cloud condensation nuclei activity, closure, and droplet growth kinetics of Houston aerosol during the Gulf of Mexico Atmospheric Composition and Climate Study (GoMACCS) *J. Geophys. Res.* **114** 1–21
Li Z, Niu F, Fan J, Liu Y, Rosenfeld D and Ding Y 2011 Long-term impacts of aerosols on the vertical development of clouds and precipitation *Nat. Geosci.,* **4** 888–94
Lin J, Pan D, Davis S J, Zhang Q, He K, Wang C and Guan D 2014 China's international trade and air pollution in the United States *Proc. Natl. Acad. Sci. U.S.A.* **111** 1736–41
Liu J, Alexander L, Fast J D, Lindenmaier R and Shilling J E 2021 Aerosol characteristics at the Southern Great Plains site during the HI-SCALE campaign *Atmos. Chem. Phys.* **21** 5101–16
Logan T, Dong X and Xi B 2018 Aerosol properties and their impacts on surface CCN at the ARM Southern Great Plains site during the 2011 Midlatitude Continental Convective Clouds Experiment *Adv. Atmos. Sci.* **35** 224–33
Logan T, Dong X, Xi B, Zheng X, Wang Y, Wu P and Maddux J 2020 Quantifying Long-Term Seasonal and Regional Impacts of North American Fire Activity on Continental Boundary Layer Aerosols and Cloud Condensation Nuclei *Earth and Space Science.* **7** 1–12
Logan T, Xi B and Dong X 2014 Aerosol properties and their influences on marine boundary layer cloud condensation nuclei at the ARM mobile facility over the Azores *J. Geophys. Res.* **119** 4859–72
Ma Y, Brooks S D, Vidaurre G, Khalizov A F, Wang L and Zhang R 2013 Rapid modification of cloud-nucleating ability of aerosols by biogenic emissions *Geophys. Res. Lett.* **40** 6293–97
Mahish M and Collins D 2017 Analysis of a multi-year record of size-resolved hygroscopicity measurements from a rural site in the U.S *Aerosol Air Qual. Res.* **17** 1489–1500
Mahish M, Jefferson A and Collins D R 2018 Influence of common assumptions regarding aerosol composition and mixing state on predicted CCN concentration *Atmosphere.* **9** 1–18
Marinescu P J, Levin E J T, Collins D, Kreidenweis S M and Van Den Heever S C 2019 Quantifying aerosol size distributions and their temporal variability in the Southern Great Plains, USA *Atmos. Chem. Phys.* **19** 11985–12006
Mei F, Hayes P L, Ortega A, Taylor J W, Allan J D, Gilman J and Wang J 2013 Droplet activation properties of organic aerosols observed at an urban site during CalNex-LA *Journal of Geophysical Research Atmospheres.* **118** 2903–17
Meng J W, Yeung M C, Li Y J, Lee B Y L and Chan C K 2014 Size-resolved cloud condensation nuclei (CCN) activity and closure analysis at the HKUST Supersite in Hong Kong *Atmos. Chem. Phys.* **14** 10267–282
Mircea M, Facchini M C, Decesari S, Cavalli F, Emblico L, Fuzzi S and Artaxo P 2005 Importance of the organic aerosol fraction for modeling aerosol hygroscopic growth and activation: A case study in the Amazon Basin *Atmos. Chem. Phys.* **5** 3111–26
Ng N L, Herndon S C, Trimborn A, Canagaratna M R, Croteau P L, Onasch T B and Jayne J T 2011 An Aerosol Chemical Speciation Monitor (ACSM) for routine monitoring of the composition and mass concentrations of ambient aerosol *Aerosol Sci. Technol.* **45** 780–94
Paasonen P, Peltola M, Kontkanen J, Junninen H, Kerminen V M and Kulmala M 2018 Comprehensive analysis of particle growth rates from nucleation mode to cloud condensation nuclei in boreal forest *Atmos. Chem. Phys.* **18** 12085–103
Parworth C, Fast J, Mei F, Shippert T, Sivaraman C, Tilp A and Zhang Q 2015 Long-term measurements of submicrometer aerosol chemistry at the Southern great plains (SGP) using an Aerosol chemical speciation monitor (ACSM) *Atmos. Environ.* **106** 43–55
Peppler R A, Bahrmann C P, Barnard J C, Campbell J R, Cheng M D, Ferrare R A and Turner D D 2000 ARM Southern Great plains site observations of the smoke pall associated with the 1998 Central American Fires *Bull. Am. Meteorol. Soc.* **81** 2563–92
Petters M D and Kreidenweis S M 2007 A single parameter representation of hygroscopic growth and cloud condensation nucleus activity – Part: II. Including solubility *Atmos. Chem. Phys.* **8** 6273–79
Pinsky M, Khain A, Mazin I and Korolev A 2012 Analytical estimation of droplet concentration at cloud base *Journal of Geophysical Research Atmospheres.* **117** 1–14
Pöhlker M L, Pöhlker C, Ditas F, Klimach T, De Angelis I H, Araújo A and Pöschl U 2016 Long-term observations of cloud condensation nuclei in the Amazon rain forest: I. Aerosol size distribution, hygroscopicity, and new model parametrizations for CCN prediction *Atmos. Chem. Phys.* **16** 15709–740
Rose D, Gunthe S S, Mikhailov E, Frank G P, Dusek U, Andreae M O and Pöschl U 2008 Calibration and measurement uncertainties of a continuous-flow cloud condensation nuclei counter (DMT-CCNC): CCN activation of ammonium sulfate and sodium chloride aerosol particles in theory and experiment *Atmos. Chem. Phys.* **8** 1153–79
Rose D, Nowak A, Achtert P, Wiedensohler A, Hu M, Shao M and Pöschl U 2010 Cloud condensation nuclei in polluted air and biomass burning smoke near the mega-city Guangzhou, China: I. Size-resolved measurements and implications for the modeling of aerosol particle hygroscopicity and CCN activity *Atmos. Chem. Phys.* **10** 3365–83
Rosenfeld D, Lohmann U, Raga G B, O'Dowd C D, Kulmala M, Fuzzi S and Andreae M O 2008 Flood or drought: how do aerosols affect precipitation? *Science* **321** 1309–13
Rosenfeld D, Andreae M O, Asmi A, Chin M, Leeuw G, Donovan D P and Quaas J 2014 Global observations of aerosol-cloud-precipitation-climate interactions *Rev. Geophys.* **52** 750–808
Schulze B C, Charan S M, Kenseth C M, Kong W, Bates K H, Williams W and Seinfeld J H 2020 Characterization of aerosol hygroscopicity over the Northeast Pacific ocean: impacts on prediction of CCN and stratocumulus cloud droplet number concentrations *Earth and Space Science.* **7** 1–26
Seinfeld J H and Pandis S N 2016 *Atmospheric Chemistry and Physics: From Air Pollution to Climate Change.* 3rd edn (New Jersey: Wiley) 978-1-118-94740-1

Seinfeld J H, Bretherton C, Carslaw K S, Coe H, DeMott P J, Dunlea E J and Wood R 2016 Improving our fundamental understanding of the role of aerosol−cloud interactions in the climate system *Proc. Natl Acad. Sci.* **113** 5781–90

Stein A F, Draxler R R, Rolph G D, Stunder B J B, Cohen M D and Ngan F 2015 Noaa's hysplit atmospheric transport and dispersion modeling system *Bull. Am. Meteorol. Soc.* (https://doi.org/10.1175/BAMS-D-14-00110.1)

Stokes G M and Schwartz S E 1994 The Atmospheric Radiation Measurement (ARM) Program: programmatic background and design of the cloud and radiation test bed *Bulletin - American Meteorological Society.* **75** 1201-1222 https://journals.ametsoc.org/view/journals/bams/75/7/1520-0477_1994_075_1201_tarmpp_2_0_co_2.xml

Swietlicki E, Hansson H C, Hämeri K, Svenningsson B, Massling A, Mcfiggans G and Kulmala M 2008 Hygroscopic properties of submicrometer atmospheric aerosol particles measured with H-TDMA instruments in various environments - A review *Tellus, Series B: Chemical and Physical Meteorology.* **60** 432–69

Trishchenko A, Luo Y, Latifovic R and Li Z 2004 Land cover type distribution over the ARM SGP area for atmospheric radiation and environmental research *Proc. of the 14th ARM Science Team Meeting (Albuquerque, New Mexico, March 22-26, 2004)*

Turpin B J and Lim H J 2001 Species contributions to pm2.5 mass concentrations: revisiting common assumptions for estimating organic mass *Aerosol Sci. Technol.* **35** 602–10

Ueda S, Miura K, Kawata R, Furutani H, Uematsu M, Omori Y and Tanimoto H 2016 Number–size distribution of aerosol particles and new particle formation events in tropical and subtropical Pacific Oceans *Atmos. Environ.* **142** 324–39

Uin J 2016 *Cloud Condensation Nuclei Particle Counter Instrument Handbook.* https://www.arm.gov/publications/tech_reports/handbooks/ccn_handbook.pdf (https://doi.org/DOE/SC-ARM-TR-168)

Wang J, Cubison M J, Aiken A C, Jimenez J L and Collins D R 2010 The importance of aerosol mixing state and size-resolved composition on CCN concentration and the variation of the importance with atmospheric aging of aerosols *Atmos. Chem. Phys.* **10** 7267–83

Wang J, Van Den Heever S C and Reid J S 2009 A conceptual model for the link between Central American biomass burning aerosols and severe weather over the south central United States *Environ. Res. Lett.* **4** 1–9

Wang Y, Wu Z, Ma N, Wu Y, Zeng L, Zhao C and Wiedensohler A 2018 Statistical analysis and parameterization of the hygroscopic growth of the sub-micrometer urban background aerosol in Beijing *Atmos. Environ.* **175** 184–191

Watson T, Aiken A, Zhang Q, Croteau P, Onasch T, Williams L and Flynn C 2018 *First ARM Aerosol Chemical Speciation Monitor Users' Meeting Report.* https://www.arm.gov/publications/tech_reports/doe-sc-arm-tr-215.pdf (https://doi.org/DOE/SC-ARM-TR-215)

Watson T, Aiken A, Zhang Q, Croteau P, Onasch T, Williams L and Flynn C 2020 *Second ARM Aerosol Chemical Speciation Monitor Users' Meeting Report.* https://www.arm.gov/publications/programdocs/doe-sc-arm-tr-249.pdf (https://doi.org/DOE/SC-ARM-TR-249)

Wex H, McFiggans G, Henning S and Stratmann F 2010 Influence of the external mixing state of atmospheric aerosol on derived CCN number concentrations *Geophys. Res. Lett.* **37** 1–4

Willis M D, Burkart J, Thomas J L, Köllner F, Schneider J, Bozem H and Abbatt J P D 2016 Growth of nucleation mode particles in the summertime Arctic: A case study *Atmos. Chem. Phys.* **16** 7663–79

Zhang F, Li Y, Li Z, Sun L, Li R, Zhao C and Fan T 2014 Aerosol hygroscopicity and cloud condensation nuclei activity during the AC3Exp campaign: Implications for cloud condensation nuclei parameterization *Atmos. Chem. Phys.* **14** 13423–437

Zhang F, Li Z, Li Y, Sun Y, Wang Z, Li P and Wang Q 2016 Impacts of organic aerosols and its oxidation level on CCN activity from measurement at a suburban site in China *Atmos. Chem. Phys.* **16** 5413–25